CHAPTER V

Fluidic-based phase reconfiguration technique using embedded slot-coupled microstrip structure

5.1. Introduction

5.2. Design and simulation

- 5.2.1. Slot coupled microstrip structure
- 5.2.2. Simulation results
- 5.2.3. Fluidic channel incorporated slot-coupled microstrip structure
- 5.2.4. Fluidic channel design and placement

5.3. Implementation and experimental validation

- 5.3.1. Fabrication process
- 5.3.2. Experimental verification of effective dielectric constant with injected DI water
- 5.3.3. Performance study of the slot-coupled microstrip structure with fluidic channels

5.4. Chapter summary

References

5.1. INTRODUCTION

This chapter presents a fluidic channel based phase reconfiguration in X-band. The proposed approach for phase reconfiguration is based on varying the extent of coupling of electromagnetic (EM) energies. The phase change is achieved by introducing a high dielectric fluid in specially designed channels within the coupling medium to vary the effective capacitance and hence the effective dielectric property. Here, effort has been made to place the fluidic channels in-situ in the coupling medium. The in-situ design of the fluidic channel based coupling media makes the the system robust, unobtrusive and overall compact. The proposed structure is simulated using CST Microwave Studio to evaluate its electromagnetic performance.

5.2. DESIGN AND SIMULATION

5.2.1. Slot-coupled microstrip structure

The prime design utilizes two broadside coupled microstrip transmission lines and placed on the opposite sides of two substrate with a slot incised in the common ground plane between the two layers of the substrate, to facilitate electromagnetic coupling between the transmission lines. The design primarily features – (1) a 50Ω transmission line patterned on the upper and lower faces of two separate substrate layers terminated in a circular patch, the circular patch is chosen to ascertain a maximum area for field accumulation in the region to achieve good coupling; and (2) a common ground plane sandwiched between the two substrates with a rectangular slot covering the circular patch region. The width, w_s, and the length, l_s, of the microstrip transmission line, and the diameter of the circular patch, D_s, directly influences the impedance of the structure and are thus optimized to get a good impedance matching at the operational frequency, refer Figure 5.1(a) . The signal can be launched at either of the ports of the microstrip structure (*say here the Port1*). The signal travelling in the top microstrip structure then couples to the below microstrip structure on the lower substrate through a rectangular aperture of length, l_e and width, w_e carved in the common ground plane as shown in Figure 5.1(b). The rectangular slot in ground plane is positioned strategically so as to align with the circular patches to intensify the electric field concentration and enable maximum slot coupling between the top and the bottom structures. The coupling is optimized by varying the dimensions of the patch and the aperture. The slot-coupled microstrip structure is designed on a $h_s = 1.27mm$ thick Rogers 5800LZ substrate with $\varepsilon_r = 2$ and $tan\delta = 0.002$. The exploded view of the design showing different layers is shown in figure 5.1(c).

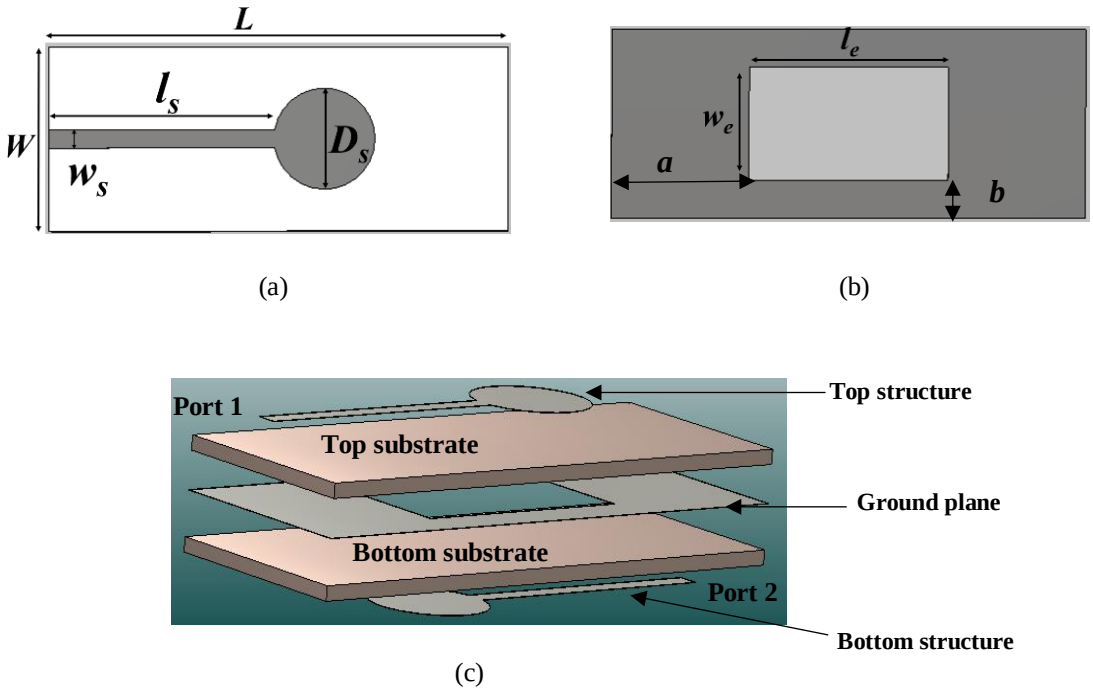

Figure 5.1. Layout of the proposed phase reconfiguration technique (a) top view showing the microstrip structure, (b) ground plane with aperture, (c) exploded view of the complete structure.

The proposed structure can be modelled as a four-port device, where, Ports 3 and 4 are open-ended, as indicated by the dotted extensions in Figure 5.2. In this configuration, Port 1 acts as the input port, through which the RF signal is launched along the top of the microstrip transmission line to the circular patch. The reflection coefficient at the open-ended Ports 3 and 4, can be assumed to be unity. The signal propagating along the top microstrip structure gets coupled to the bottom circular patch through the slot aperture and transmit to Port 2.

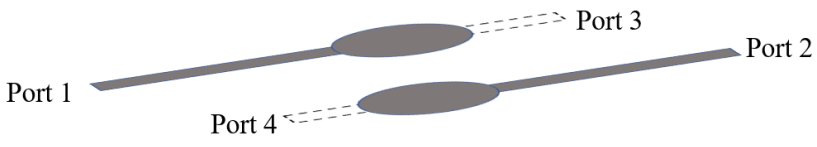

Figure 5.2. Proposed phase reconfiguration structure as a four-port network.

5.2.2. Simulation results

The key parameters, return loss, S_{11} and insertion loss, S_{21} are calculated at the input Port 1and output Port 2, respectively. In this work, a reference frequency of 10.5 GHz is

considered for analysis. As illustrated in Figure 5.3, the design demonstrates a good impedance matching, achieving a return loss better than -10 dB from 9.8GHz and across the X-band range. Further, an insertion loss of -1.4 dB is observed at 10.5 GHz, indicating effective signal transmission through the slot coupled structure.

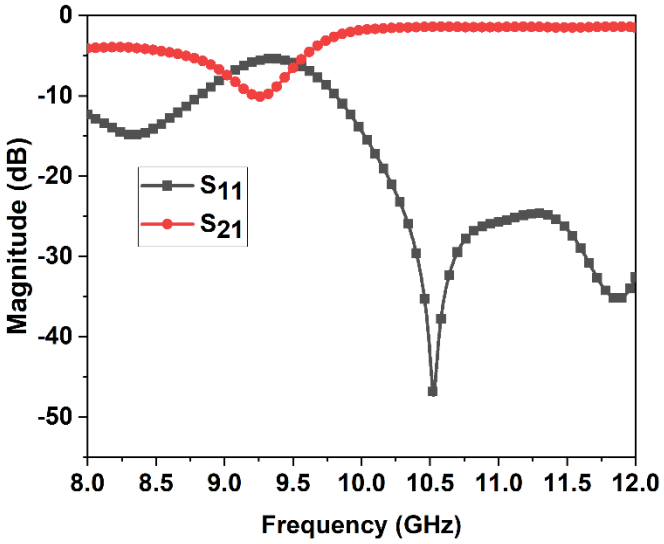

Figure 5.3. Simulated performance, S_{11} and S_{21} of the slot coupled microstrip structure.

5.2.3. Fluidic channel incorporated slot-coupled microstrip structure

The phase of the signal received at the output port in a slot coupled microstrip topology is influenced by the intensity of coupling between the top and the bottom transmission structures via the aperture in the ground plane. The intensity of coupling is indicated by a parameter called the coupling factor, C. The phase reconfiguration can be achieved by adjusting C between the two transmiting structures. The coupling factor primarily depends on the physical dimensions of the slot aperture and the dielectric properties of the coupling region, as illustrated in figure 5.1(c). Unlike altering the physical dimensions, as done in reference [1], here, the value of C is altered by modifying the effective dielectric constant of the coupling medium using fluids of higher dielectric constants. A thin epoxy layer with $\varepsilon_r = 3.4$ and $tan\delta = 0.05$ is introduced between the upper and lower substrate which serves as the structural base for incorporating the fluidic channels. Figure 5.4(a) shows lateral view of placement of the epoxy layer. The epoxy layer of height, $h_{ep} = 2.5mm$, is taken so as during fabrication the fluidic channels can be easily incorporated. The return

loss and insertion loss of the slot-coupled microstrip line structure with the introduced epoxy layer is plotted in Figure 5.4(b). The proposed design shows a simulated -10dB impedance bandwidth ranging from 10.07-11.06 GHz with an insertion loss of -2.75dB at 10.5GHz. Compared to the results obtained without the epoxy layer, refer Figure 5.3, the presence of epoxy layer results in decrease of return loss bandwidth and corresponding increase in insertion loss. The reason for this change could be because of the higher dielectric constant of the epoxy as compared to the substrate. The optimized dimension of the design with the epoxy layer is placed in Table 5.1.

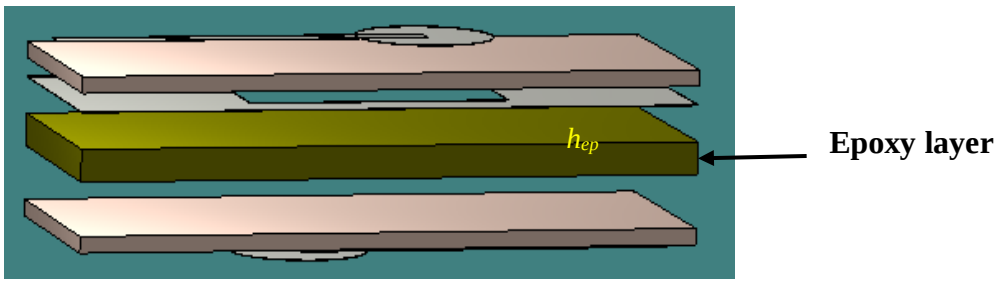

(a)

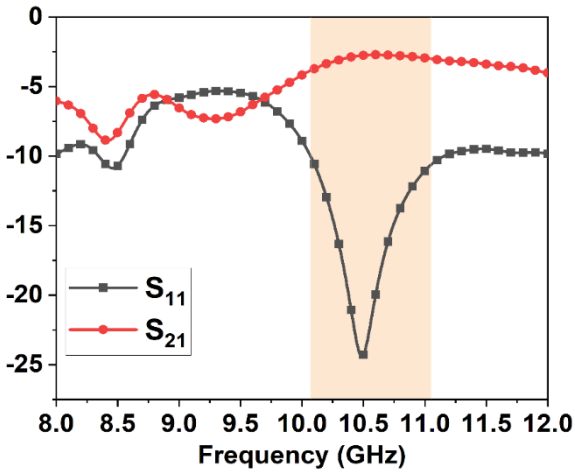

(b)

Figure 5.4. (a) Lateral schematic view of placement of epoxy layer between the substrates. (b) Simulated S_{11} and S_{21} of the structure with epoxy layer.

Table 5.1. Optimized parameters of the proposed phase reconfiguration structure at 10.5GHz

Parameter	L	W	D_s	L_s	l_e	w_e	w_s	h_s	h_{ep}	a	b
Dimensions (mm)	50	20	11	24.5	19	10	2	1.27	2.5	14.5	4

5.2.4. Fluidic channel design and placement

Fluid selection and its microwave characterization

The fluid to be chosen for phase tuning must have sufficiently high dielectric constant to effectively manipulate the dielectric constant of the medium, be less volatile at room temperature, less costly and non-toxic. Fluids like hexanol, toluene, FC-77, liquid crystals and liquid metal have been previously used for reconfigurable RF devices but the constrain being the cost and availability [2-5]. In this work, deionized (DI) water is used for phase reconfiguration due to its high dielectric permittivity, non-toxic nature, low cost, and widespread availability, making it an effective and safe choice for prototyping tunable fluidic-based RF applications. Permittivity studies in the X-band are carried out on deionized (DI) (Thermo Fisher Scientific India Pvt. Ltd.), water at room temperature ($\sim 25°C$) using a dielectric probe kit (Keysight N1501A) compatible with a PNA series Agilent Vector Network Analyzer E8362C (VNA). The permittivity and loss tangent are plotted in Figure 5.5(a) and (b). The dielectric permittivity value of DI water at $10.5\ GHz$ is measured as $\varepsilon' = 68.7$, with a corresponding $tan\delta \sim 0.12$.

(a)

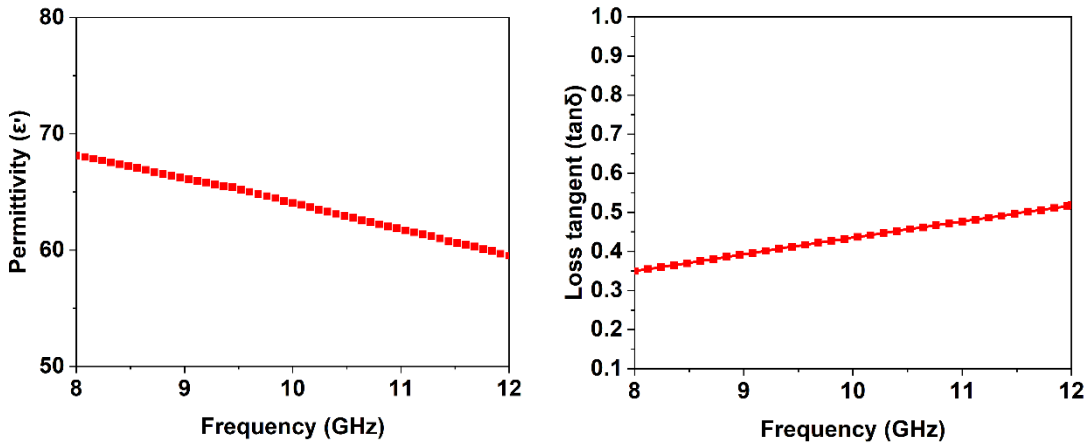

(b) (c)

Figure 5.5 (a) Dielectric characterization setup using dielectric probe kit. Measured (b) permittivity, ε' and (c) $tan\delta$, of DI water.

Placement of fluidic channel

Phase reconfiguration using a fluidic mechanism is implemented by using eight parallel fluidic channels of diameter, $d_f = 1\,mm$, and integrated into the structure. These channels are uniformly distributed with an inter-channel spacing of $s = 2\,mm$, such that they span almost over the entire rectangular aperture area of the ground plane, enabling strong electromagnetic interaction between the guided wave and the dielectric fluid, as illustrated in schematic Figure 5.6. The selection of the channel dimensions and their spacing is driven primarily by practical fabrication constraints. The fluidic channels are activated in a controlled way to ensure symmetry in the electromagnetic response and to maintain a balanced phase shift behavior. Table 5.2 shows the fluid-injection modes in the eight-channel structure, where white cells represent air-filled and blue cells represent water-filled channels. Mode 1 corresponds to all-air channels, while Modes 2–5 progressively increase the number of water-filled channels from the center outward, with Mode 5 representing the fully filled case.

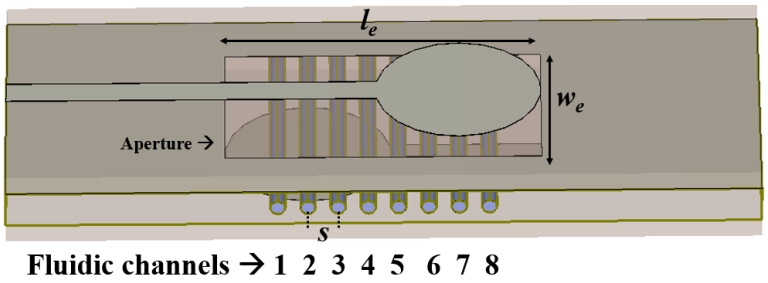

Figure 5.6 Schematic view of the placement of the fluidic channels in the epoxy layer.

Table 5.2. Modes of fluid injection in the fluidic channel

Fluidic channels									
1	**2**	**3**	**4**	**5**	**6**	**7**	**8**		
								Mode 1	**All channels filled with air**
								Mode 2	**Channel 4 and 5 filled with DI water**
								Mode 3	**Channel 3, 4, 5 and 6 filled with DI water**
								Mode 4	**Channel 2, 3, 4, 5, 6 and 7 filled with DI water**
								Mode 5	**All channels filled with DI water**

Air filled Water filled

Performance study for different modes of fluid injection

The simulated behaviour of the design in terms of its transmission amplitude, S_{21}, and phase characteristics for different modes are shown in Figure 5.7. At $10.5GHz$, a total phase shift of 37° is observed with a maximum insertion loss of -4.34dB with all channels filled i.e. Mode 5 configuration. The phase reconfiguration is achieved in 5 discrete states depending upon the different modes of fluid injection in the channels.

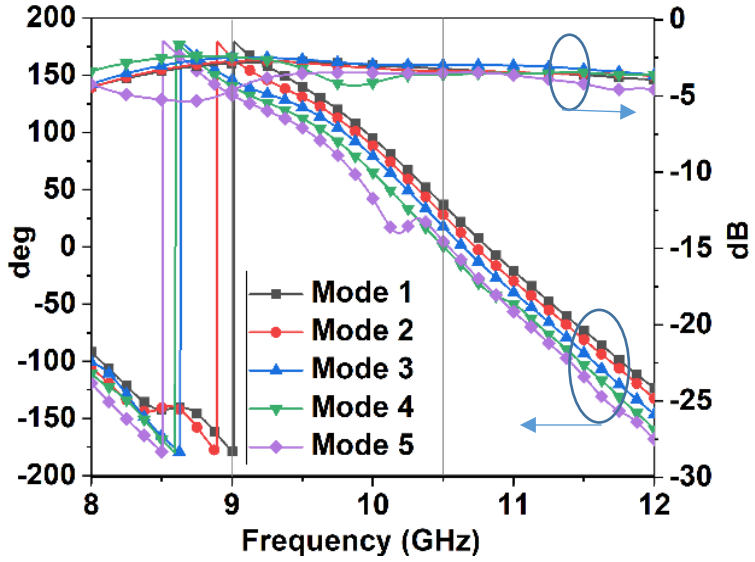

Figure 5.7 Simulated phase changes and insertion loss for different modes of fluid injection in the channel.

The phase variation in the signal can be explained based on the phase delay in the signal propagating along the transmission lines and determined using Equation 5.1.

$$\Delta\varphi = \frac{\omega L_{TL}}{v_p} \qquad (5.1)$$

where, Δ φ is the phase shift, ω is the angular velocity, L_{TL} is the effective length of the transmission lines and v_p, is the phase velocity.

The phase velocity can be further expressed as Equation 5.2 [8]

$$v_p = \frac{\sqrt{2}}{\sqrt{\mu\varepsilon}} \frac{1}{\sqrt{1+\sqrt{1+\frac{\sigma^2}{\omega^2\epsilon^2}}}} \qquad (5.2)$$

where, μ is magnetic permeability, ε is dielectric permittivity and σ is electric conductivity of the transmitting medium. At higher frequencies, the effect of electric conductivity can be neglected, which modifies Equation 5.2 to,

$$v_p = \frac{\sqrt{2}}{\sqrt{\mu\varepsilon}} \qquad (5.3)$$

From Equation 5.3, it can be seen that the phase velocity, v_p is dependents on the permittivity, ε , and permeability, μ ,of the medium. The operating technique of the design can be explained from equations (5.1) and on (5.3), i.e. by altering the effective dielectric constant of the medium, the phase velocity can be modified, causing a corresponding alteration in the phase value of the propagating signal.

Field analysis

The cross-sectional schematic of the proposed slot-coupled fluidic phase reconfiguration structure is illustrated in Figure 5.8(a). Visualization of the electromagnetic behavior under different reconfiguration states are presented in Figures 5. 9(b) and (c), showing electric field distribution for the orthogonal cross-sections of the design, corresponding to Mode 1 and Mode 5 , respectively. The electric field is predominantly concentrated in the substrate

region, between the two broadside-coupled microstrip lines, directly beneath the ground plane aperture indicated by high intensity red arrows. This region is of critical interest, as it coincides with the embedded fluidic channels, thereby enabling direct interaction between the propagating electromagnetic fields and the tunable dielectric medium.

In Mode 1, with all the channels filled with air, the field distribution exhibits a baseline intensity governed by the substrate's intrinsic permittivity and the air-filled channels. However, in Mode 5, when DI water is introduced into all the channels, a noticeable enhancement in the local electric field intensity is observed. The high permittivity of DI water ($\varepsilon_r = 68.7$), contributes in increasing the effective dielectric constant in the coupling region. The elevated permittivity results in stronger confinement, thereby intensifying the electromagnetic interaction between the coupled lines as observed in Figure 5.9(c).

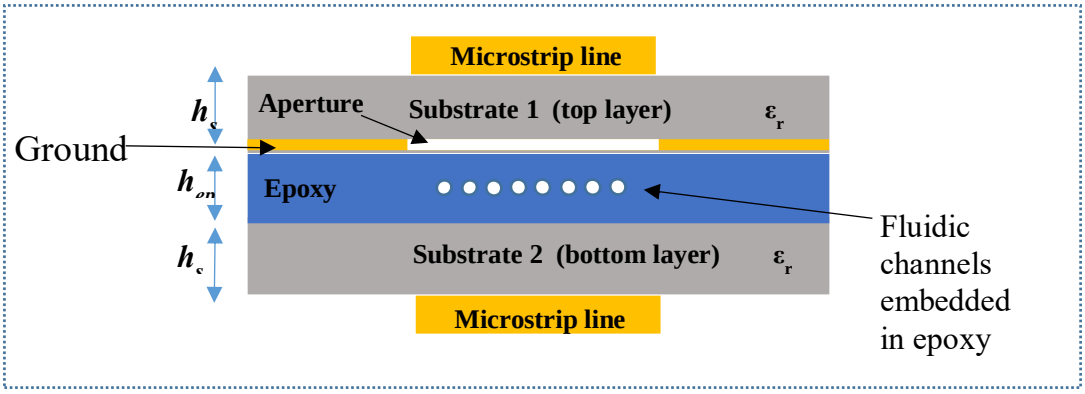

(a)

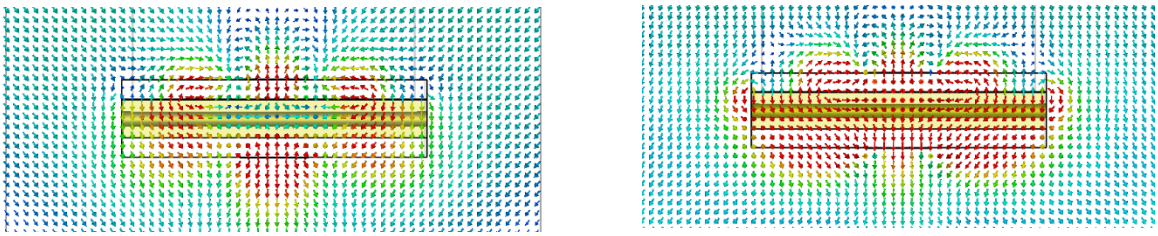

(b) (c)

Figure 5.8. (a) Schematic of cross-sectional view of the design showing different layers. (b) E-field distribution with all channels air filled, Mode 1 and (c) E- field distribution with all channels filled with DI water, Mode 5.

5.3. IMPLEMENTATION AND EXPERIMENTAL VALIDATION

5.3.1. Fabrication process

The fabrication process of slot-coupled fluidic phase reconfigurable design involves two steps *viz.* preparation of the substrate with printed microstrip structured geometries and realization of the fluidic channels in the sandwiched epoxy layer.

Substrate preparation

The top and bottom microstrip structures are fabricated using chemical etching. The metallic traces of microstrip lines with circular patch terminations are patterned onto one side of two Rogers 5880LZ substrates, each with a thickness of 1.27 mm and a relative permittivity, $\varepsilon_r = 2$, as per the specifications listed in Table 5.1. Other side of one of the substrate is selectively etched to form a ground plane (*here the top layer*) with a rectangular aperture of dimensions $l_e \times w_e$, as per the dimensions specified in Table 5.1 and placed underneath the circular patch to enable maximum electromagnetic coupling through the slot. On other hand the metal backing of the other substrate is etched completely, so as to get only single ground plane.

Epoxy-based fluidic channel realization

The intermediate epoxy layer for holding the fluidic channels is fabricated using additive manufacturing techniques combined with epoxy casting. A mould is first created using polylactic acid (PLA) and 3D printed to match the planar dimensions of the substrate and vertical height, $h_{ep} = 2mm$, corresponding to the required thickness of the epoxy layer. The internal channel geometry is created with eight steel needles of diameter $d_f = 1mm$ inserted horizontally through the sidewalls of the PLA mould at its mid-height. The needles are spaced evenly with an inter-channel distance, $s = 2\,mm$, as illustrated in Figure 5.10(a). The epoxy layer is formed using EPOKE Art Epoxy Resin. Prior to casting, the resin is degassed in a vacuum desiccator to eliminate entrapped air bubbles, which could otherwise impact the electromagnetic performance. The degassed resin is slowly poured into the mould to ensure uniform filling and is then left to cure undisturbed for 72 hours at ambient conditions as shown in Figure 5.10(b). The photograph of cured epoxy with fluidic channel is given in Figure 5.10(c). The top and bottom substrates are aligned and bonded

on either side of the epoxy layer to complete the tri-layer assembly. Sub-miniature type A (SMA) connectors are soldered to the microstrip lines to facilitate signal feeding and receiving as shown in Figure 5.10(d). The lateral view of the final assembled prototype, is presented in Figures 5.10(e).

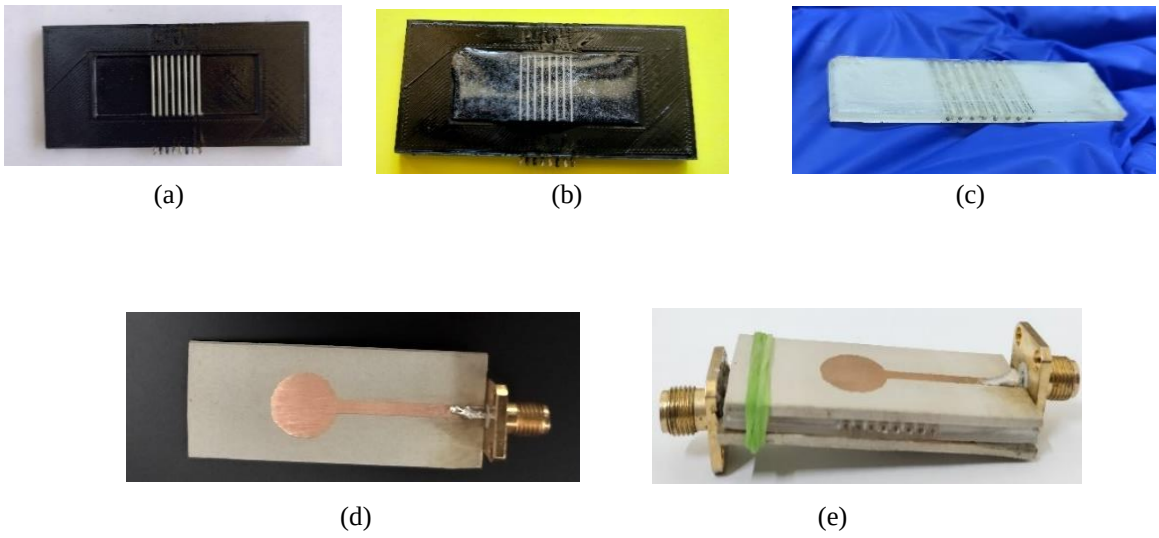

(a) (b) (c)

(d) (e)

Figure 5.9 (a) Steel needles inserted in 3D printed PLA mould. (b) Epoxy resin poured in the mould and left to cure. (c) Cured epoxy layer with fluidic channels. (d) Metallic trace of the microstrip line with circular patch termination. (e) Lateral view of assembled prototype.

5.3.2. Experimental verification of effective dielectric constant with injected DI water

The effect of deionized (DI) water injection on the effective permittivity is experimentally checked with transmission–reflection method using Nicholson-Ross-Weir (NWR) technique. Epoxy substrate with a single fluidic channel engraved, is placed in a waveguide adapter setup. The test sample has dimension similar to Agilent WR-90 X11644A waveguide i.e. $22.86 \times 10.16\ mm^2$ compatible with the Agilent E8362C Vector Network Analyzer (VNA). The sample is placed inside a waveguide sample holder as shown in Figure 5.11(a). The complex permittivity ($\varepsilon_r = \varepsilon_r' - j\varepsilon_r''$) of the material in the X-band frequency range (8.2–12.4 GHz) is determined using the Agilent 85071E material measurement software, which applies the Nicolson-Ross-Weir (NRW) method [14,15]. Measurements are conducted using a vector network analyzer (VNA) connected to the waveguide ports as shown in Figure 5.8(a-b). Two sets of measurements are performed:

- Air-filled single channel configuration.
- DI water-filled single channel configuration.

The results are presented in Figures 5.8(c and d), showing a comparison of the extracted permittivity, ε' , and $tan\delta$ for both the configurations. From Figure 5.11(b), the analysis reveals that the epoxy substrate with an air-filled channel exhibited an effective relative permittivity of approximately 2.9. On injecting DI water ($\varepsilon' \approx 68.7$) into the fluidic channel, the effective permittivity increased to 3.2. This change demonstrates that the introduction of a high-permittivity fluid within the fluidic channels leads to a measurable increase in the overall dielectric constant of the composite structure. As shown in Figure 5.11(d), the loss tangent values of the material remain largely unaffected by the injection of the fluid, indicating minimal impact on dielectric losses.

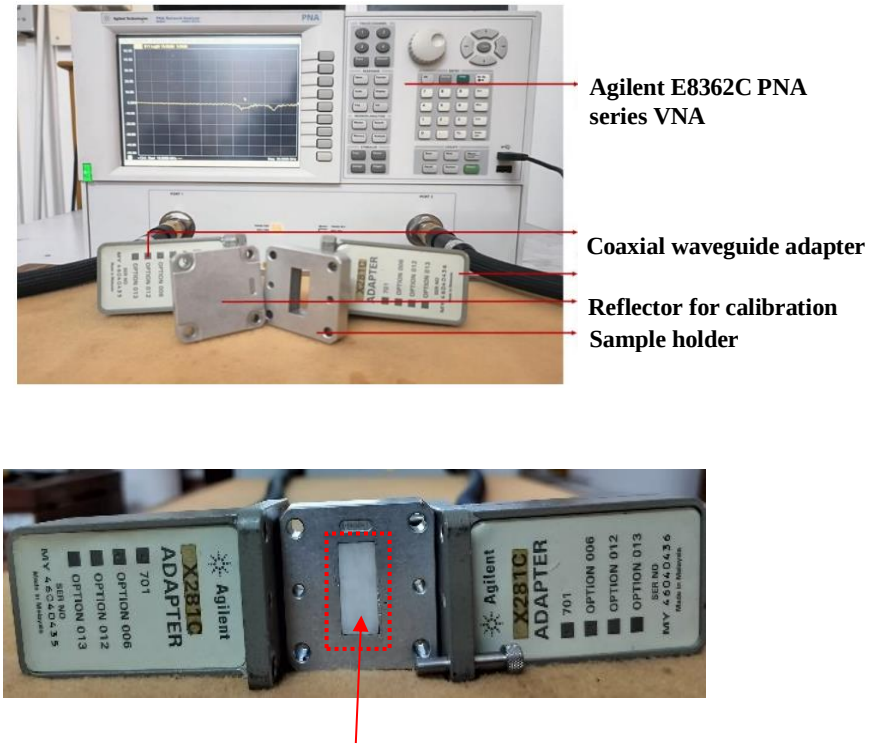

(a)

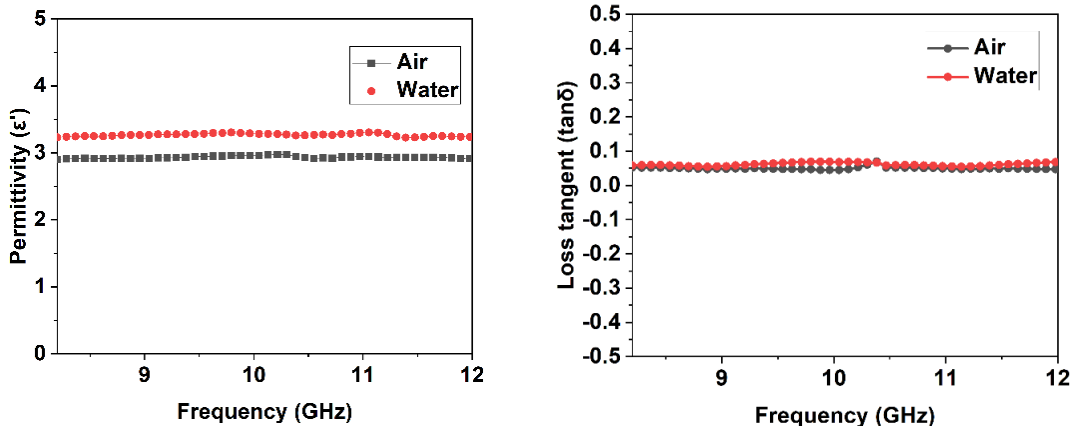

(b) (c)

Figure 5.10 (a) Dielectric characterization setup with fluidic channel incorporated epoxy substrate placed in the waveguide adapter. Measured (a) permittivity, ε' and (b) loss tangent, $tan\delta$ of epoxy substrate prototype.

The permittivity values from the above studies are tabulated in Table 5.3

Table 5.3 Measured dielectric constants and loss tangents

Material	**Dielectric constant**	**Loss tangent**
DI water	68.7 ± 0.06	0.457 ± 0.024
Epoxy with single air filled fluidic channel	2.83 ± 0.08	0.051 ± 0.006
Epoxy with single DI filled fluidic channel	3.2 ± 0.04	0.055 ± 0.019

5.3.3. Performance study of the slot-coupled microstrip structure with fluidic channels

The performance of fabricated prototype shown in Figure 5.10(e) is studied for its return loss, S_{11}, and insertion loss, S_{21}, using Agilent Vector Network Analyzer E8362C (VNA) calibrated through Agilent 85052D calibration kit as shown in Figure 5.12(a) described in Chapter III. The desired quantity of DI water (Thermo Fisher Scientific India Pvt. Ltd.), is injected in the fluidic channels using a micropipette as illustrated in figure 5.12(b). One end of the channel is sealed using a thin layer of hot glue to avoid water to drain out from the it. The fluid is then filled in accordance with different modes as described in Table 5.2.

(a)

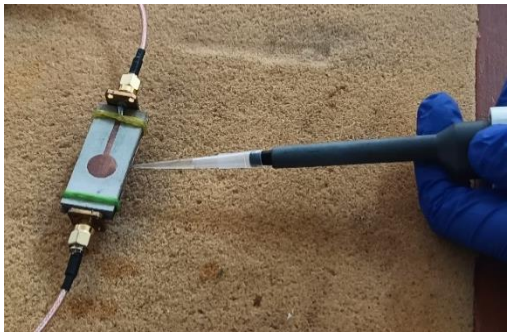

(b)

Figure 5.11. (a) Fabricate prototype connected to VNA for S_{21} measurement. (b) Photograph of injection of DI water inside the fluidic channel using micropipette.

Figures 5.13 (a), (b), and (c) plots S_{11}, S_{21} and transmission phase shift for various DI water injection modes respectively. At the reference frequency of 10.5 GHz, the insertion loss for Mode 1 is measured as -3.06 dB, while Mode 5 configuration exhibits a maximum insertion loss of -4.92 dB. Across the five discrete fluidic states, a total phase tuning range of 43.8° is achieved. Table 5.4 presents a detailed comparison of phase shifts and corresponding insertion losses for each mode. The observed trend confirms that an increasing number of water-filled channels enhances the effective dielectric constant and hence the coupling capacitance between the microstrip structures. This leads to a progressive decrease in phase values. The behavior aligns with a previous findings reported in [2] where similar dielectric-dependence phase tuning is observed using different fluidic materials.

The reusability of the design is investigated by removing the fluid from all the channels and re-performing the measurement. The device is returned to its initial state after draining out all the water from all the channels indicated by Mode 1´. A small phase deviation of

0.99° is observed compared to the original air-filled configuration i.e. Mode 1 is observed. The reusability is repeated multiple times, and the maximum deviation is plotted. The plots coincide as can be seen from Figure 5.13(d). This confirms the reliability, reusability, and stability of the design under multiple tuning cycles.

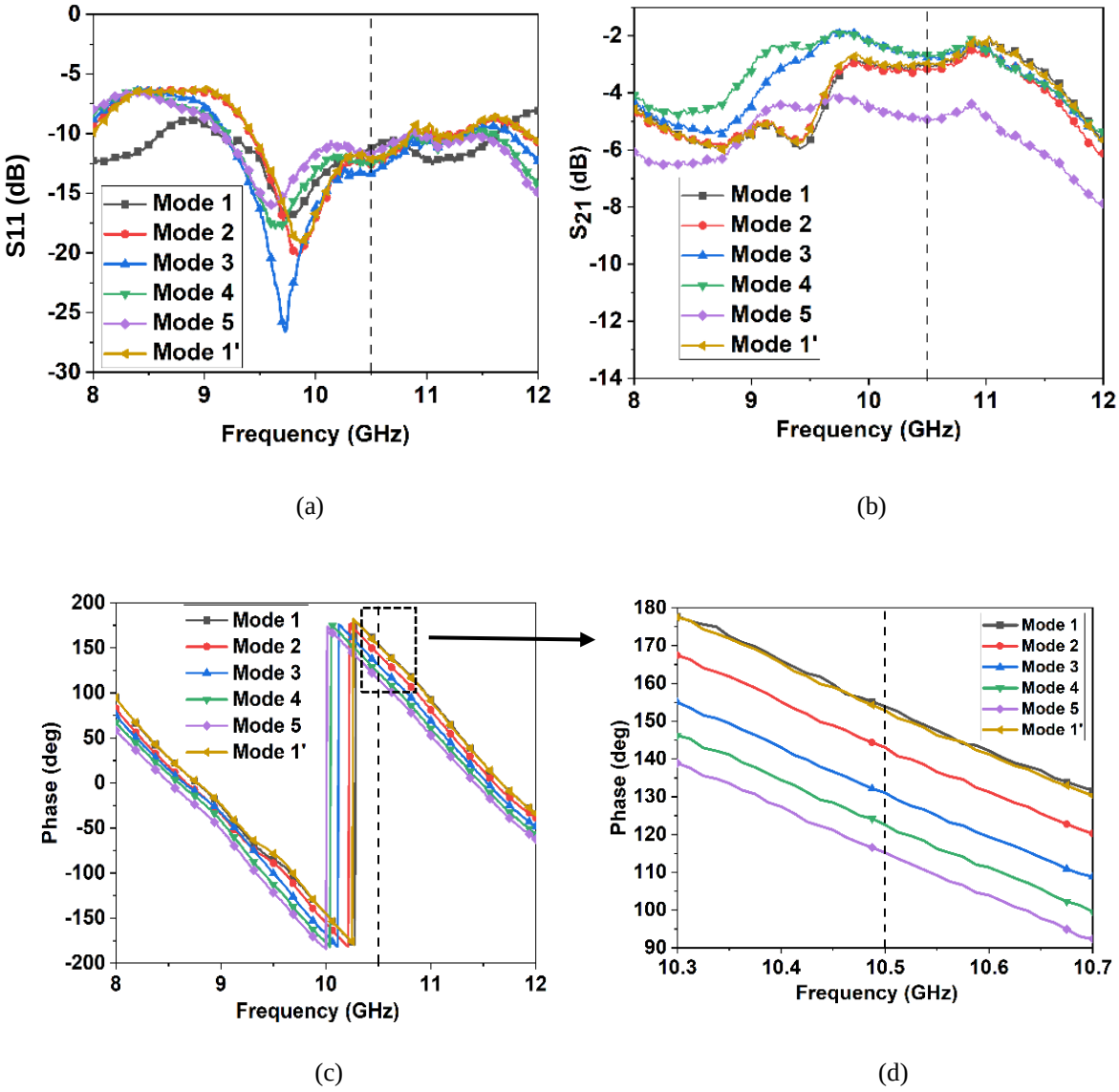

Figure 5.12 Measured (a) return loss, S_{11}, (b) insertion loss, S_{21} and (c) phase shifts for different modes of fluid injection. (d) Expanded region of the plot at 10.5GHz.

Table 5.4 Performance of the proposed design at 10.5GHz in terms of insertion loss and phase shift for different mode of fluid injection

Modes of fluid injection	Insertion loss (dB)		Phase shift (deg)	
	Simulated	**Measured**	**Simulated**	**Measured**
Mode 1	-2.9	-3.06	-	-
Mode 2	-2.7	-3.17	8.83	10.79
Mode 3	-2.5	-2.76	10.40	12.10
Mode 4	-2.45	-2.65	17.15	11.91
Mode 5	-4.04	-4.92	7.30	9.0
Mode 1'	-	-2.98	-	0.99

5.4. CHAPTER SUMMARY

This chapter presents a fluidic-based dynamic phase reconfiguration technique for X-band applications, offering a compact, low-cost, and reliable solution. The proposed design employs vertically coupled microstrip transmission lines integrated with fluidic channels for phase reconfiguration. Fluidic channels are embedded in-situ within an epoxy substrate that is sandwiched between the two coupled strip lines. The overall design measures 20 mm × 50 mm × 5.1 mm and provides a cost-effective approach by utilizing de-ionized (DI) water as the tuning fluid. The technique eliminates the need for external biasing circuitry and active components, ensuring simple and low-power operation. Placement of the fluidic channels inside the substrate not only simplifies fabrication but also shields the channels from external damage, overcoming the limitation of [9] where exposed channels were more vulnerable. The high dielectric permittivity of DI water alters the effective permittivity of the substrate, resulting in a shift in the output signal phase. Experimental validation shows a maximum phase shift of 43.8° at 10.5 GHz, realized in five discrete phase states, while the insertion loss ranges from –2.65 dB to –4.92 dB at the same frequency. Reusability tests confirm a negligible phase deviation of 0.99° compared to the initial value. Continuous phase tuning is also feasible by precisely controlling the volume of fluid within the channels, highlighting the flexibility and robustness of the proposed design.

References

[1]. Abbosh, A. M. Ultra-Wideband Phase Shifters. *IEEE Transactions on Microwave Theory and Techniques*, 55(9):1935–1941, 2007. DOI: 10.1109/TMTT.2007.904051

[2]. Choi, S., Su, W., Tentzeris, M. M., & Lim, S. A novel fluid-reconfigurable advanced and delayed phase line using inkjet-printed microfluidic composite right/left-handed transmission line. *IEEE Microwave and Wireless Components Letters*, 25(2):142–144, 2015. DOI: 10.1109/LMWC.2014.2382685

[3]. Wu, Y.-W., Tang, S.-Y., Churm, J., & Wang, Y. Liquid metal-based tunable linear phase shifters with low insertion loss, high phase resolution, and low dispersion. *IEEE Transactions on Microwave Theory and Techniques*, 71(9):3968–3978, 2023. DOI: 10.1109/TMTT.2023.3248954

[4]. Qaroot, A., & Mumcu, G. Microfluidically reconfigurable reflection phase shifter. *IEEE Microwave and Wireless Components Letters*, 28(8):684–686, 2018. DOI: 10.1109/LMWC.2018.2847046

[5]. Sun, S.-Y., et al. Electronically tunable liquid-crystal-based F-band phase shifter. *IEEE Access*, 8:151065–151071, 2020. DOI: 10.1109/ACCESS.2020.3017165

[6]. Weir, W. B. Automatic measurement of complex dielectric constant and permeability at microwave frequencies. *Proceedings of the IEEE*, 62(1):33–36, 1974. DOI: N/A

[7]. Nicolson, A. M., & Ross, G. F. Measurement of the intrinsic properties of materials by time-domain techniques. *IEEE Transactions on Instrumentation and Measurement*, 19(4):377–382, 1970. DOI: N/A

[8]. Balanis, C. A. *Advanced Engineering Electromagnetics*. John Wiley & Sons, New York, NY, USA, 1989. DOI: N/A.

[9]. Choi, S., Su, W., Tentzeris, M. M., and Lim, S. A Novel Fluid-Reconfigurable Advanced and Delayed Phase Line Using Inkjet-Printed Microfluidic Composite Right/Left-Handed Transmission Line. *IEEE Microwave and Wireless Components Letters*, 25(2):142–144, Feb. 2015. DOI: 10.1109/LMWC.2014.2382685